Journal of Computer Aided Diagnosis of Medical Images Vol.2 Oct. 1998

Original Paper

A Method for Automatic Detection of Spicules in Mammograms

Hao JIANG*, Wilson TIU**, Shinji YAMAMOTO** and Shun-ichi IISAKU*

Abstract: This paper presents a method for automatic detection of spicules in mammograms. The method consists of two steps, enhancement and feature selection. First, spicule shadows are enhanced by a newly developed operation. An opening operation is applied to remove noise and a direction map is made for feature selection. Second, a concentration expression is given with gray levels and two features are selected for recognition of tumors with spicules. In the method, not only is the direction of spicules considered, but also the density is utilized. The method was tested on 24 samples which included seven tumors with spicules. The recognition rate for tumors with spicules was 100% without false positives.

Key words: medical image, mammogram, automatic detection, mathematical morphology

1. Introduction

Breast cancer is one of the leading cancers in the female population. Mammographic screening is the most effective method of early detection; however, manually reading mammograms is labor intensive. Several approaches to analyzing mammograms by computer have been proposed in the past [Brzakovic 90, Dhawan 86, Dengler 93, Dhawan 96, Highnam 94, Kegelmeyer 92, Kegelmeyer 93, Kobatake 96, Karssemeijer 96, Lai 89, Laine 94, Morrow 92, Ng 92, Petrick 96, Qian 94, Spiesberger 79, Shen 94, Strickland 96, Sahiner 96, Zheng 96]. These approaches can be loosely grouped into two categories, approaches for identifying clustered microcalcifications [Dengler 93, Dhawan 96, Spiesberger 79, Strickland 96, Zheng 96] and approaches for tumor detection [Brzakovic 90, Kegelmeyer 92, Kegelmeyer 93, Kobatake 96, Karssemeijer 96, Lai 89, Ng 92, Petrick 96, Sahiner 96].

Since the existence of spicules is one of most important visual signs in diagnosing breast cancer, several of these studies discuss the detection of tumors with spicules [Ng 92, Kegelmeyer 92, Kegelmeyer 93, Kobatake 96, Karssemeijer 96]. A spine-oriented method for the recognition of tumor with spicules has been presented by Ng [Ng 92]. Kegelmeyer suggested an approach to detecting spicules based on analyses of local oriented edges [Kegelmeyer 92, Kegelmeyer 93]. Kobatate proposed a method for detecting spicules based on skeleton analyses and Hough transformation [Kobatake 96]. And finally, a method of detecting stellate distortions based on statistical analyses of maps of pixel orientations has been proposed by Karssemeijer [Karssemeijer 96]. All of the studies suggested that the direction of spicules is useful information for detecting of tumors with spicules.

This paper describes a method for automatically recognizing spicule shadows in mammograms. The method considers not only the direction of spicules, but also the density for classifying tumors with spicules. In the next section, we give an overview of the method. Section 3 discusses a method for enhancing spicule shadows, which is modified based on gray scale reconstruction of mathematical morphology and preserves gray levels of spicule shadows. In Section 4, two features are provided for classification of spicule shadows from others such as blood vessels and mammary glands. Experimental results as well as the results of a comparison with thresholding are given in Section 5.

2. Method overview [Jiang 97a, Jiang 97b]

Most breast carcinomas appear as stellate lesions, consisting of a central tumor mass surrounded by spicules. Spicules have a star-shaped structure that emanates from the central mass with sharp, dense, and fine lines. A model

*Communications Research Laboratory, MPT
(Koganei, Tokyo 184-8795, Japan)
**Toyohashi University of Technology
(Toyohashi, Aichi 441, Japan)
received: 1 July 1998
revised: 6 October 1998
accepted: 7 October 1998

of a spicule is illustrated in **Fig. 1** and is considered as a ridge. The central tumor mass is an isolated shadow and appears as a bright blob on mammograms. Candidate shadows of central tumor masses can be detected by using the method proposed by Yamamoto [Yamamoto 96]. In this method, input images for recognition of spicules are separated from original images based on the detected locations of candidate central tumor masses. A flowchart of the recognition process for spicules is shown in **Fig. 2**.

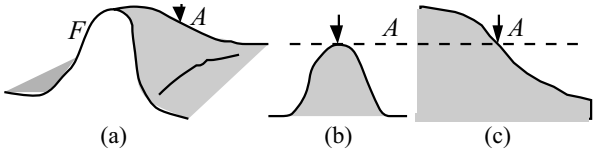

Fig. 1 The model of a spicule shadow,
(a) a bird's eye view with gray levels,
(b) gray levels intersecting spicule at *A*,
(c) gray levels along with spicule at *A*.

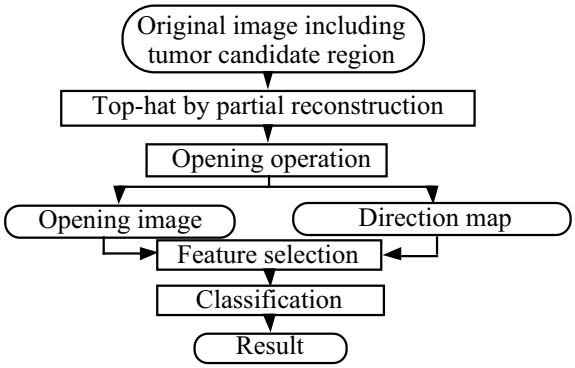

Fig. 2 Flowchart for recognition of spicules

The spicule recognition method we propose consists of two steps, enhancement of spicule shadows and feature selection. First, spicule shadows are enhanced by using a newly developed operation. An opening operation is applied to remove noise and a direction map is made for feature selection. Then, a concentration expression of spicules around a central mass candidate region is given with gray levels and two features are selected based on the expression for classification.

3. Enhancement of spicules

A new operation, called top-hat by partial reconstruction (*TPR*), is proposed for enhancing the image of the spicules. This operation is based on gray scale reconstruction of mathematical morphology [Vincent 93]. In this section, we first review gray scale reconstruction and provide a modified gray scale reconstruction, i.e., gray scale partial reconstruction and *TPR*. Then we apply an opening operation to remove noise and make a direction map of spicules for the next step of classification.

3.1 Gray scale reconstruction

Vincent provided two definitions of gray scale reconstruction [Vincent 93]. Let F and S be two gray scale images defined on the same domain and $S(p) < F(p)$ for each pixel p. The gray scale reconstruction R can be given by

$$R(S) = \{ I_{n+1} = (I_n \oplus B) \wedge F, \text{ until } I_{n+1} = I_n \} \qquad (1)$$

where $I_n \oplus B$ is the dilation of I_n by structuring element B, $I_0 = S$, and $\wedge$ stands for pointwise minimum.

The gray scale reconstruction R of F from S is obtained by iterating gray scale geodesic dilations of S under F until stability is reached. The regional domes of image F can be extracted by subtracting the reconstructed image from the original image; i.e., the components with high frequency can be effectively detected based on the gray scale reconstruction. This operation is called top-hat by reconstruction.

On the other hand, spicules are the components with high frequency, but the lines with directions. So that it is difficult to extract spicules by gray scale reconstruction because two dimensional flat structuring elements are used in the definitions. For example, **Fig.3** illustrates gray scale reconstruction applied to a spicule. At point *A*, the peak does not appear in the cross section along the spicule in **Fig.1**(c), although it does appear in the cross section intersecting the spicule in **Fig.1**(b). The top of the spicule (broken line of **Fig.3**(c)) can be extracted, but the shoulder with the higher gradient can not be extracted and is reconstructed by iterating gray scale geodesic dilations.

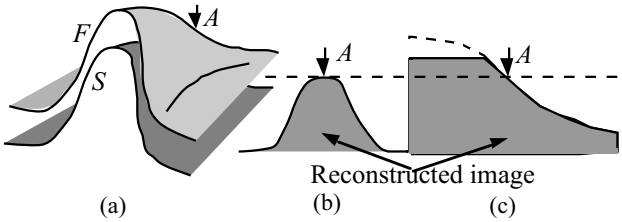

Fig. 3 Gray scale reconstruction of spicule shadow,
(a) bird's eye views of *F* and *S* with gray levels,
(b) gray levels intersecting spicule shadow at *A*,
(c) gray levels along with spicule shadow at *A*.

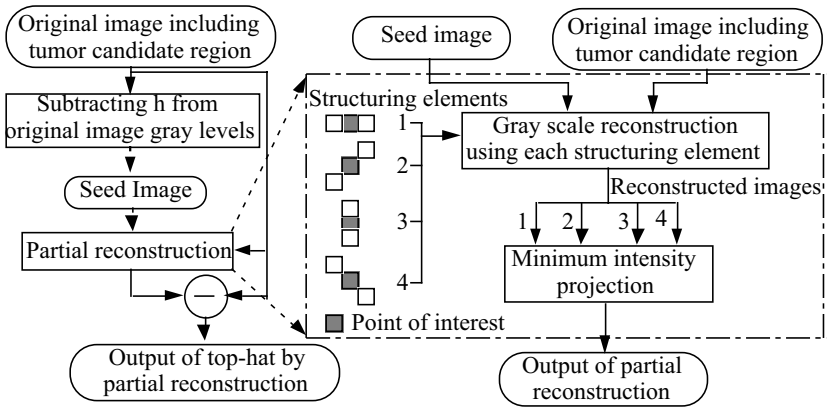

Fig. 4 Top-hat by partial reconstruction

3.2 Top-hat by partial reconstruction

Since spicules are long and slender shadows and have directions, the operation for enhancing spicule shadows is based on gray scale reconstruction that preserves the direction, length and density of spicules. The operation is shown in **Fig. 4**. The modified gray scale reconstruction, i.e., gray scale partial reconstruction *PR*, is given by

$$PR = Min \{ R_k (S, B_k) \} \quad (k = 1, 2, 3, 4) \qquad (2)$$

where B_k is structuring element with direction as shown in **Fig. 5** and *Min* is minimum operation. The top-hat by partial reconstruction *TPR* is given by

$$TPR = F - PR. \qquad (3)$$

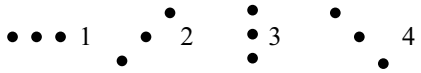

Fig. 5 The structuring elements of four directions for gray scale partial reconstruction

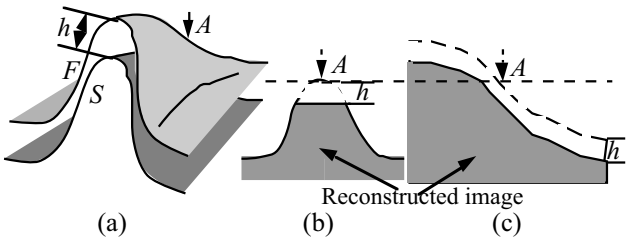

Fig. 6 Gray scale partial reconstruction,
(a) bird's eye views of *F* and *S* with gray levels,
(b) gray levels intersecting spicule at *A*,
(c) gray levels along spicule at *A*.

Fig. 6 illustrates the *TPR* operation. Let us first prepare four different structuring elements (**Fig. 5**) and generate a seed image *S* by subtracting a constant *h* from original image *F*. We then carry out the gray scale reconstruction for each structuring element and operate pointwise minimum of the four reconstructed images to obtain *PR*. Finally, we subtract the image of *PR* from the original image *F* to enhance the spicules so that they are below the gray level *h*. For example, at point *A* in **Fig. 6**, the output of the *PR* operation using the structuring element, which is parallel to the spicule, is higher than that of the other three structuring elements. The original image is reconstructed (just like the gray scale reconstruction of **Fig. 3**(c)). However, the output using the structuring element, which is perpendicular to the spread direction of the spicule, is lower. Therefore, the spicule shadows are enhanced and the difference *h* is preserved by minimum and *TPR* operations (**Fig. 6**).

3.3 Seed image selection

The seed image *S* uses the image subtracted from the original image with constant *h* because it can be automatically obtained and the details of the spicules are preserved. So that the seed image is included in the original image and the gray levels of the spicules enhanced by *TPR* operation are restricted to be below *h*. In our experiments, *h* is selected based on the gray levels measured from spicules in the original images.

3.4 Opening operation and direction map

After the *TPR* operation, an opening operation is applied to suppress noise and a direction map is made for classifying tumors with spicules. A flowchart showing the opening operation and direction map generation is shown in **Fig. 7**.

The structuring element of opening is eight bars with different directions and the length of bars is experimentally determined to remove noise and preserve the enhanced spicules. The opening operation is carried out by using each structuring element and an opening image is obtained by pointwise maximum of intensities from the eight images.

Eight direction codes are given according to eight structuring elements with different directions as shown in

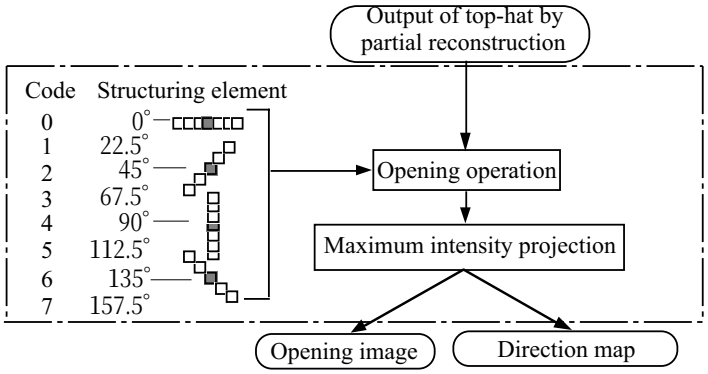

Fig.7 Opening operation and direction map

Fig. 7. If a maximum output of the opening operation using a structuring element is obtained from outputs of the opening operation using eight structuring elements at a pixel, the direction code of the structuring element is considered as a direction unit vector of a spicule at the pixel and recorded in the direction map (**Fig. 7**).

4. Feature selection and classification

In this section, we give the concentration expression of spicules based on the enhanced image and direction map and select two features for classification.

4.1 Concentration expression of spicules

Let S_i express the degree of concentration of spicules for a selected region *i*, which can be given by

$$Si = \sum_{m,n} Si\,(m,n) \tag{4}$$

$$Si\,(m,n) = \frac{\sum_{x,y} \frac{\cos\alpha \cdot bo\,(x,y)}{r}}{\sum_{x,y} \frac{bo\,(x,y)}{r}} \tag{5}$$

where *bo*(x,y) is the gray level of pixel (x,y), α is the angle between the line from pixel (m,n) to (x,y) and the direction unit vector at pixel (x,y), and *r* is the distance between pixel (m,n) and (x,y).

Term S_i is measures the concentration behavior of the radiating line pattern around a central region. The term cosα is a measure of the convergence from pixel (x,y) to pixel (m,n). If it is close to 1.0, it means that the direction vector points to the pixel (m,n) (**Fig. 8**(a)). The direction map is applied to calculate cosα. The term *bo*(x,y) is the gray level of spicule at pixel (x,y) and is the output of the opening operation. The term *1/r* is the amount the influence of the pixel is suppressed as the distance increases. The denominator of equation 5 normalizes the degree bounded between 0 and 1.0.

4.2 Mask selection

Two masks are selected for classification of spicules. One is for the concentration region of spicules and the other is for the existence region. The concentration region is the domain of pixel (m,n) and the area of a circle with radius r_1 from central point *O* of the tumor candidate region, which is previously determined. The value of r_1 is experimentally determined. The discussion with respect to r_1 is also in the following section. The existence region is the domain of point (x,y) and the bounded area of circles from radius r_1 to r_2. The radius r_2 is also experimentally determined, but it is large enough to include the central mass and spicules.

4.3 Classification

To suppress the reflections of noise such as from blood vessels and fibrous tissues, the existence region is not directly used to calculate the degree of concentration. Instead, the existence region is partitioned into eight small regions R_i (i=1,⋯,8) having the same size (**Fig. 8**(b)) and the degree of concentration of each region S_i (i=1,⋯,8) is calculated individually by equations (4) and (5). Then two features are selected to classify spicules and others such as blood vessels and mammary glands.

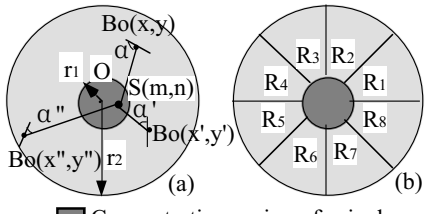

Concentration region of spicules
Existence region of spicules
(a) Two masks of concentration and existence regions of spicules
(b) 8 small regions partitioned from existence region of spicules

Fig. 8 The masks and regions for feature selection

Let us denote the mean and the minimum of S_i by S_{mean} and S_{min}. The two features are given as

$$S_{mean} = (S_1+S_2+\cdots+S_8)/8 \quad (6)$$

$$S_{min} = Min\ (S_1,S_2,\cdots,S_8) \quad (7)$$

where *Min* is minimum operation. It is clear that the values of S_{mean} and S_{min} are close and large for spicules and the values are small for others such as blood vessels and mammary glands.

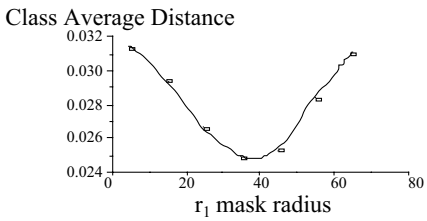

Fig. 9 Relationship between the mask radius of concentration region and average distance in class.

5. Experiments

5.1 Experimental data set

The mammograms used in the experiments are computed radiography (CR) images from a data base published by the Japan Society of Computer Aided Diagnosis of Medical Images. The spatial resolution is 0.1 mm and the size of each CR image is 2550×2100 pixels with 10-bit accuracy. We used 24 samples to evaluate the performance of the proposed method. The original images of the samples are partitioned 512×512 sized areas based on the positions of candidate regions identified as containing central tumor masses [Yamamoto 96]; i.e., seven samples that include tumors with spicules, five samples that include tumors without spicules, eight samples of mammary glands, and four samples of blood vessels.

5.2 Experimental conditions

The position of a candidate region of a central tumor mass is first detected by using Quoit filtering [Yamamoto 96]. Quoit filtering is effective for detecting isolated shadow-like central tumor masses.

The *h* of generating seed image is 10 for enhancement of spicules and the value is the mean of gray levels of 10 places selected from the original images with spicules. The length of the bar filter used in the opening operation is 20 pixels. The radii r_1 and r_2 of the mask radius are respectively 38 and 200 pixels. The central point *O* is the center of gravity of the tumor candidate region. The radius r_2 is determined based on the consideration that the maximum diameter of concentric circles formed by spicules is less than 40 mm. The value of r_1 is experimentally determined based on the following discussion.

The features of S_{mean} and S_{min} are calculated from samples with spicules by changing the value r_1. The average of distance in the class of tumors with spicules is calculated based on the two features. **Fig. 9** shows the result and there is a minimum at r_1=38; i.e., for the optimal classification of tumors with spicules, the radius r_1 should be 38 pixels.

5.3 Results

Fig. 10 shows a series of images for classification based on the proposed method. **Fig. 10**(a) is the input image and is enhanced by *TPR* processing as shown in **Fig. 10**(b). The gray levels of the image are bounded from 0 to 10. The values of spinal axes of spicules and local maxima are close to 10. The result of opening operation is shown in **Fig. 10**(c) and the noises such local maxima are mostly suppressed. **Fig. 10**(d) shows the direction code at each pixel in the direction map for the right lower frame in **Fig. 10**(c). The code corresponds to the direction code of **Fig. 8**. The code at a pixel is the mean, if the number of the code with the same maximum in opening operations of eight directions is appeared in multiple times from 2 to 4. The sign - means that there is not a spicule pixel and the - is given if the number of the code with the same maximum is appeared more than 5 times among eight directions of opening operation. **Fig. 10**(e) and (f) are the two masks, one for the concentration region and one for the existence region.

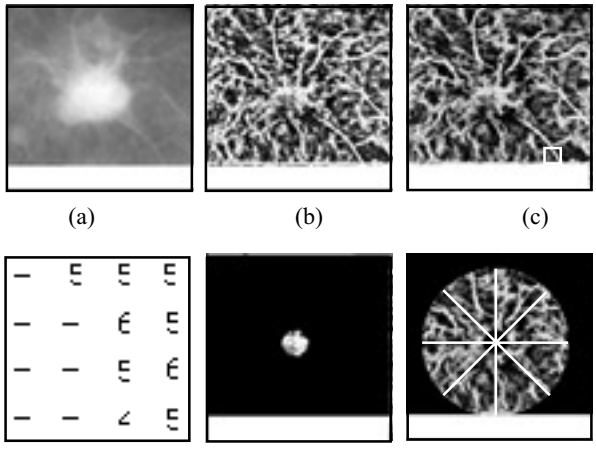

Fig. 10 Series of images for recognition of spicules,
(a) original image,
(b) enhancement,
(c) opening operation,
(d) direction map,
(e) concentration region of spicules,
(f) partitioned existence region.

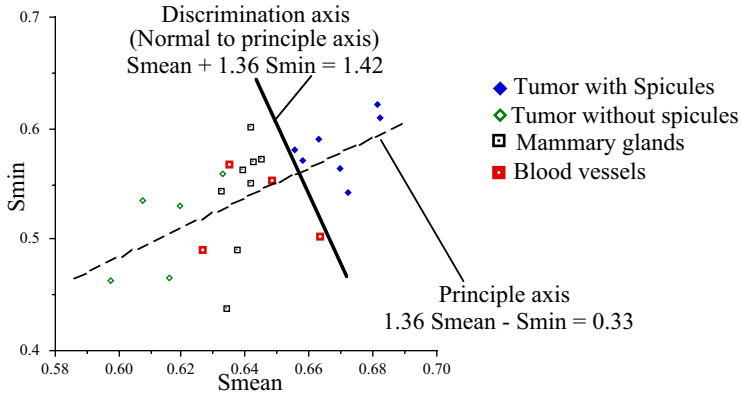

Fig. 11 Classification graph

Table 1 Classification results

Input images \ Classification	Tumors with spicules	The others
Tumors with spicules	7/7	0/7
The others	0/17	17/17

The experimental results for the 24 samples are shown in **Fig. 11** (the axes are S_{mean} and S_{min}). Tumors with spicules and others such as blood vessels and mammary glands are classified according to the following condition. The sample is classified as a tumor with spicules if the features S_{mean} and S_{min} are respectively larger than 0.652 and 0.521. **Table 1** shows the classification results for this condition.

The discrimination function is normal to the principle axis obtained based on the two features and is given by

$$S_{mean} + 1.36\, S_{min} = 1.42. \qquad (8)$$

5.4 Discussion

In equation (5), not only is the direction of spicules considered, but also the gray level of each pixel for feature selection. The effectiveness of introducing gray levels of the enhanced spicules is discussed as follows.

An appropriate threshold is selected for the binarization of the enhanced spicules, which is 8 in our experiments. Other conditions are the same as the experiments above. The experimental results shown in **Fig. 12** clearly show that the separation between the sets of tumors with spicules and other sets such as blood vessels and mammary glands is not good, i.e., it is difficult to find a function that classifies them. It can be found from the original images and the enhanced images that there are small spicules with weak contrast around the central mass. Therefore, the threshold selection is very difficult and the gray levels are important for classifying tumors with spicules.

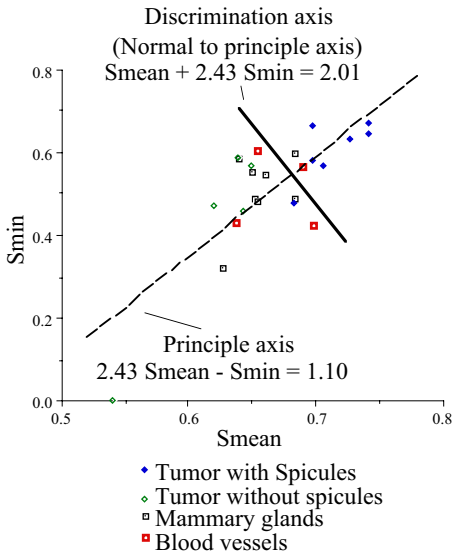

Fig. 12 Classification graph using a binarized image

6. Conclusion

In this paper, a method for automatic detection of spicules in mammograms has been proposed. The spicule shadows are first enhanced by using a newly developed operation called top-hat partial reconstruction. The operation can preserve the length of spicules. An opening operation is applied to remove noise and a direction map is made for

feature selection. Next, a spicule concentration expression is given and two features are selected for classification that characterize the radiating structure of spicule shadows. Not only is the direction of spicule shadows considered but also the density is utilized for classification of tumors with spicules. Experiments to test the performance of the proposed method have been presented. Twenty-four samples including seven tumors with spicules have been classified perfectly without false positives. In the next step, we will increase the number of samples considerably to verify the robustness of the proposed method, and evaluate the performance in comparison with other methods.

References:

[Brzakovic 90] D. Brzakovic, X.M. Luo, and P. Brzakovic: An approach to automated detection of tumors in mammograms, IEEE Trans. Med. Imaging, Vol. MI-9, No. 3, pp. 233-241, 1990

[Dhawan 86] A.P. Dhawan, G. Buelloni, and R. Gordon: Enhancement of mammographic features by optimal adaptive neighborhood image processing, IEEE Trans. Med. Imaging, Vol. MI-5, No. 1, pp. 8-15, 1986

[Dengler 93] J. Dengler, S. Bebine, and J.F. Desaga: Segmentation of microcalcifications in mammograms, IEEE Trans. Med. Imaging, Vol. MI-12, No. 4, pp. 634-642, 1993

[Dhawan 96] A.P. Dhawan, Y. Chitre, C. Kaiser-Bonasso, and M. Moskowitz: Analysis of mammographic microcalcifications using gray-level image structure features, IEEE Trans. Med. Imaging, Vol. MI-15, No. 3, pp. 246-259, 1996

[Highnam 94] R.P. Highnam, J.M. Brady, and B.J. Shepstone: Computing the scatter component of mammographic images, IEEE Trans. Med. Imaging, Vol. MI-13, No. 2, pp. 301-313, 1994

[Jiang 97a] H. Jiang, W. Tiu, S. Yamamoto, and S. Iisaku: Automatic recognition of spicules in mammograms, Proc. of 9th ICIAP, LNCS 1311, Springer, pp. 396-403, 1997

[Jiang 97b] H. Jiang, W. Tiu, S. Yamamoto, and S. Iisaku: Detection of spicules in mammograms, Proc. of IEEE ICIP-97, Vol. III, pp. 520-523, 1997

[Kegelmeyer 92] W.P. Kegelmeyer, Jr.: Computer detection of stellate lesions in mammograms, Proc.'92 SPIE Conf. on Biomedical Image Processing and 3-D Microscopy, Vol.1660, pp. 446-454, 1992

[Kegelmeyer 93] W.P. Kegelmeyer, Jr.: Evalution of stellate lesion detection in a standard mammogram data set, in K.W. Bowyer and S. Astley eds: State of the art in digital mammographic image analysis, World Sientific, pp. 262-279, 1993

[Kobatake 96] H. Kobatake and Y. Yoshinaga: Detection of spicules on mammograms based on skeleton analysis, IEEE Trans. Med. Imaging, Vol. MI-15, No. 3, pp. 235-245, 1996

[Karssemeijer 96] N. Karssemeijer, and G.M.te Brake: Detection of stellate distortion in mammograms, IEEE Trans. Med. Imaging, Vol. MI-15, No. 5, pp. 611-619, 1996

[Lai 89] S.-M. Lai, X. Li, and W.F. Bischof: On techniques for detecting circumscribed masses in mammograms, IEEE Trans. Med. Imaging, Vol. MI-8, No. 4, pp. 377-386, 1989

[Laine 94] A.F. Laine, S. Schuler, J. Fan, and W. Huda: Mammographic feature enhancement by multiscale analysis, IEEE Trans. Med. Imaging, Vol. MI-13, No. 4, pp. 725-740, 1994

[Morrow 92] W.M. Morrow, R.B. Paranjape, R.M. Rangayyan, and J.E.L. Desautels: Region-based contrast enhancement of mammograms, IEEE Trans. Med. Imaging, Vol. MI-11, No. 3, pp. 392-406, 1992

[Ng 92] S.L. Ng, and W.B. Bischof: Automated detection and classification of breast tumors. Computers and Biomedical Research, Vol. 25, pp. 218-237, 1992

[Petrick 96] N. Petrick, H.-P. Chan, B. Sahiner, and D. Wei: An adaptive density-weighted contrast enhancement filter for mammographic breast mass detection, IEEE Trans. Med. Imaging, Vol. MI-15, No. 1, pp. 59-67, 1996

[Qian 94] W. Qian, L.P. Clarke, M. Kallergi, and R.A. Clark: Tree-structured nonlinear filters in digital mammography, IEEE Trans. Med. Imaging, Vol. MI-13, No. 1, pp. 25-36, 1994

[Spiesberger 79] W. Spiesberger: Mammogram inspection by computer, IEEE Trans. Biomed. Engin., Vol. BME-26, No. 4, pp. 213-219, 1979

[Shen 94] L. Shen, R.M. Rangayyan, and J.E.L. Desautels: Application of shape analysis to mammographic calcifications, IEEE Trans. Med. Imaging, Vol. MI-13, No. 2, pp. 263-274, 1994

[Strickland 96] R.N. Strickland, and H.I. Hahn: Wavelet transforms for detecting microcalcifications in mammograms, IEEE Trans. Med. Imaging, Vol. MI-15, No. 2, pp. 218-229, 1996

[Sahiner 96] B. Sahiner, H.-P. Chan, N. Petrick, D. Wei, M.A. Helvie, D.D. Adler, and M.M. Goodsitt: Classification of mass and normal breast tissue: A convolution neural network classifier with spatial domain and texture images, IEEE Trans. Med. Imaging, Vol. MI-15, No. 5, pp. 598-610, 1996

[Vincent 93] L. Vincent: Morphological Grayscale Reconstruction in Image Analysis: Applications and Efficient Algorithms, IEEE Trans. Image Processing, Vol. IP-2, No. 2, pp. 176-201, 1993

[Yamamoto 96] S.Yamamoto, M.Matsumoto, Y.Tateno, T.Iinuma, and T.Matsumoto: Quoit filter -- a new filter based on mathematical morphology to extract the isolated shadow, and its application to automatic detection of lung cancer in X-ray CT, Proc. of 13th ICPR, Vol. II, pp. 3-7, 1996

[Zheng 96] B.Zheng, W.Qian, and L.P.Clarke: Digital mammography: Mixed feature neural network with spectral entropy decision for detection of microcalcifications, IEEE Trans. Med. Imaging, Vol. MI-15, No. 5, pp. 589-597, 1996

Authors:

Hao JIANG received his B.S. in mechanical engineering from Hefei University of Technology, China in July 1982 and his Ph.D. in information engineering from Nagoya University in May 1992. From June 1992 to March 1996, he was an assistant professor at Toyohashi University of Technology. From April 1996, he joined the Communications Research Laboratory, Ministry of Posts and Telecommunications, as a senior researcher. His research interests are image processing, pattern recognition, graphics, virtual reality, and applications in medicine.

Wilson TIU received his B.S. and M.S. degrees in knowledge based information engineering from Toyohashi University of Technology in March 1993 and March 1995, respectively. Since April 1995, he has been with the Yutaka Co. Ltd. His interests are image processing and its application to medical image.

Shinji YAMAMOTO received his B.S. and Ph.D. degrees in electronics engineering from Nagoya University in March 1962 and March 1974, respectively. From April 1962 to August 1973 he was a researcher, and from August 1973 to February 1980, he was a senior researcher at the Central Research Laboratory, Hitachi Co. Ltd.. From February1980 to February 1987, he was the director of the Medical Engineering Research Division at the Central Research Laboratory, Hitachi Co. Ltd, and from February 1987 to March 1990, he was the director of the Development Division at the Naka Factory of Hitachi Co. Ltd.. From April 1990, he joined the Toyohashi University of Technology as a professor. His research interests are image processing, pattern recognition, applications in medicine, character recognition, and applications to handwriting characters.

Shin-ichi IISAKU received his Ph.D. from Hokkaido University in 1982. He joined Kokusai Denshin Denwa Co., Ltd., where he worked in the R&D labs and his interests were network architecture and communication protocols. In 1995, he joined the Communications Research Laboratory, Ministry of Posts and Telecommunications. His research interests are intelligent multimedia retrieval and image processing.

Journal of Computer Aided Diagnosis of Medical Images Vol.2 Oct. 1998

乳房Ｘ線像におけるスピキュラ陰影自動認識の一手法

江　　浩*　テュ　ウィルソン**　山本眞司**　飯作俊一*
*郵政省通信総合研究所，**豊橋技術科学大学

本論文では乳房Ｘ線像におけるスピキュラ陰影自動認識の一手法について述べる. 本手法はスピキュラ陰影強調処理と特徴量選択という二つのステップからなっている. まずスピキュラ陰影の強調処理を行う. その強調処理では，Mathematical Morphologyを用いたTophat by Partial Reconstructionという新しく開発した手法を用いる. またその強調処理で得られた画像に対して雑音除去及びスピキュラの伸びる方向を示す方向マスクを作成する. そしてその画像における各画素の濃淡値及び方向を用いてスピキュラの集中度を計算し, 二つの特徴量を選択して識別関数を作り，入力画像におけるスピキュラ陰影の有無を自動認識する．実験ではスピキュラ陰影を有する７症例を含む２４症例に本手法を適用した結果，全て正しく認識された.